Particle & Particle Systems Characterization
www.particle-journal.com

Temperature Dependence of Water Absorption in the Biological Windows and Its Impact on the Performance of Ag_2S Luminescent Nanothermometers

Tamara Muñoz-Ortiz, Lise Abiven, Riccardo Marin, Jie Hu, Dirk H. Ortgies, Antonio Benayas, Florence Gazeau, Victor Castaing, Bruno Viana, Corinne Chanéac, Daniel Jaque, Fernando E. Maturi, Luís D. Carlos, Emma Martín Rodríguez, and José García Solé*

The application of nanoparticles in the biological context generally requires their dispersion in aqueous media. In this sense, luminescent nanoparticles are an excellent choice for minimally invasive imaging and local temperature sensing (nanothermometry). For these applications, nanoparticles must operate in the physiological temperature range (25–50 °C) but also in the near-infrared spectral range (750–1800 nm), which comprises the three biological windows of maximal tissue transparency to photons. In this range, water displays several absorption bands that can strongly affect the optical properties of the nanoparticles. Therefore, a full understanding of the temperature dependence of water absorption in biological windows is of paramount importance for applications based on these optical properties. Herein, the absorption spectrum of water in the biological windows over the 25–65 °C temperature range is systematically analyzed, and its temperature dependence considering the coexistence of two states of water is interpreted. Additionally, to illustrate the importance of state-of-the-art applications, the effects of the absorption of water on the emission spectrum of Ag_2S nanoparticles, the most sensitive luminescent nanothermometers for in vivo applications to date, are presented. The spectral shape of the nanoparticles' emission is drastically affected by the water absorption, impacting their thermometric performance.

1. Introduction

The first systematic report on the temperature dependence of liquid water absorption in the near-infrared (NIR) was published in 1925.[1] In that work, it was already proposed that the complex spectrum of water results from the coexistence of two kinds of water molecules (or water states) whose relative concentration depends on the temperature. This interpretation was based on the assumption given by Röntgen in 1892 to explain the anomalous properties of liquid water.[2] Röntgen denoted the water molecules belonging to these two states as *water molecules* and *ice molecules*. At that time, it was supposed that they were related to single water molecules (called hydrol) and aggregates of two or three molecules (called dihydrol or trihydrol, respectively). The simultaneous presence of these molecules should contribute to the experimentally observed broadening of the

T. Muñoz-Ortiz
Instituto Investigación Sanitaria Princesa (IIS-IP)
Universidad Autónoma de Madrid
Calle Diego de León, 62, Madrid 28006, Spain

T. Muñoz-Ortiz, R. Marin, D. H. Ortgies, A. Benayas, D. Jaque, E. Martín Rodríguez, J. García Solé
Nanomaterials for bioimaging group (NanoBIG)
Facultad de Ciencias
Universidad Autónoma de Madrid
C/ Francisco Tomás y Valiente 7, Madrid 28049, Spain
E-mail: emma.martin@uam.es

The ORCID identification number(s) for the author(s) of this article can be found under https://doi.org/10.1002/ppsc.202200100.

DOI: 10.1002/ppsc.202200100

L. Abiven, C. Chanéac
Sorbonne Université
CNRS
Collège de France
LCMCP
Place Jussieu 4, Paris 75005, France

L. Abiven, V. Castaing, B. Viana
IRCP
PSL Chimie ParisTech
CNRS
Rue P. & M. Curie 11, Paris 75005, France

L. Abiven, F. Gazeau
Université Paris Diderot
CNRS
MSC
Rue Alice Domon et Léonie Duquet 10, Paris 75013, France

J. Hu
Xiamen Institute of Rare-earth Materials
Haixi Institutes
Chinese Academy of Sciences
Duishanxiheng Road 258, Jimei District Xiamen, Fujian 361024, China

Particle & Particle Systems Characterization
www.particle-journal.com

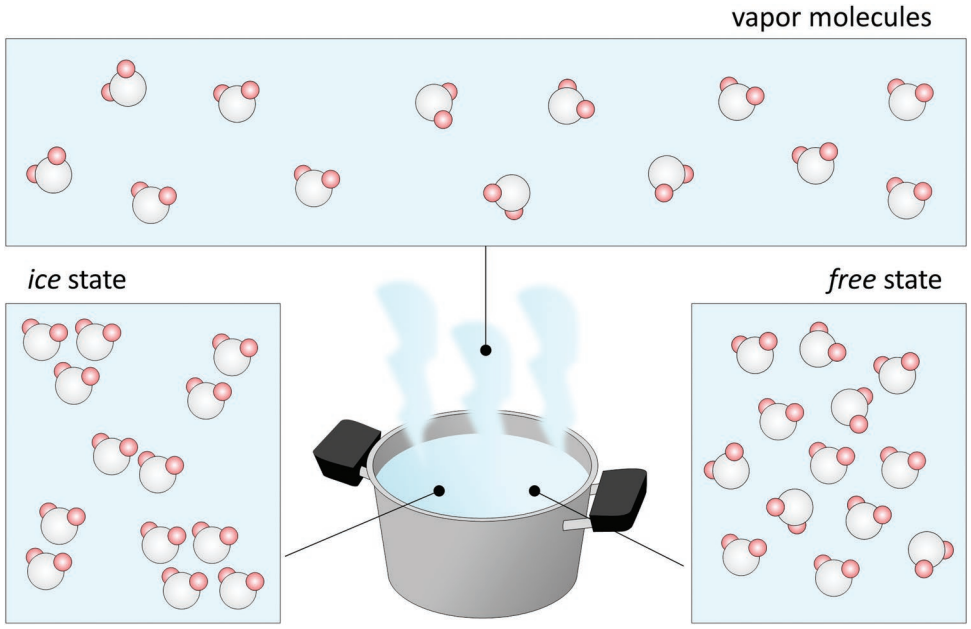

Figure 1. Schematic (artistic) representation of the two kinds of water states coexisting in liquid water. Molecules in the ice state should belong to ordered structures (small clusters), while molecules in the free state should be almost free molecules, close to the ones observed in the vapor state.

absorption bands in the liquid state compared to the vapor state spectrum. As the temperature rises, the relative amount of water molecules should increase at the cost of ice molecules, determining the temperature dependence of the peak position, shape, and intensity of most absorption bands in liquid water. Although several works have dealt with the spectrum of liquid water in different spectral regions,[3] the number of those dealing with the spectral range encompassing the biological windows (NIR-I: 750–950 nm, NIR-II: 1000–1350 nm, NIR-III: 1500–1800 nm[4]), where the luminescence of most of the nanoparticles for deep tissue imaging occurs, is still scarce.[5] In addition, the temperature dependence of the main absorption bands in this spectral range has also been barely analyzed.[1,5c,6] As practically all nanoparticle-based applications use water or water-based solutions as dispersants, it is evident that a careful analysis of the temperature dependence of the main absorption bands of liquid water in the biological windows is of paramount importance. In fact, these bands can dramatically affect the emission spectra of the nanoparticles due to an inner absorption filter effect.

As predicted by Röntgen, nowadays it is widely accepted that the molecules of liquid water display at least two different structural arrangements (water states) in the physiological range of temperature.[7] Despite the nature of these states still being a matter of debate, plenty of information has been obtained concerning the structure and arrangement of water molecules in both states.[7c,8] **Figure 1** illustrates the two water states, which were herein labeled as *ice* state and *free* state, departing slightly from the terms *ice molecules* and *water molecules* adopted by Röntgen just to avoid chemical misinterpretations. Indeed, recently reported experimental results have confirmed that, in the simplest approach, liquid water consists of two water states.[8,9] At temperatures close to 0 °C the water molecules mainly form clusters of few molecules, giving an average dipole moment of 2.8 D for each water molecule. This scenario corresponds to the *ice* state in Figure 1. As the temperature is raised, these clusters are being decoupled to form free molecules (*free* state) with a much lower average dipole moment of 1.8 D.[10]

Within this simple scheme, the molecules in the *ice* state should be dominating at room temperature, while molecules in the *free* state should predominate at temperatures close to the boiling point (100 °C in pure water). As a matter of fact, several physicochemical properties of liquid water show a change in the behavior at temperatures around 40–50 °C.[9–11] The temperature at which these changes occur has been lately labeled crossover temperature. At temperatures below the crossover point, water molecules are mostly arranged in organized clusters (*ice* state) while above the crossover temperature these clusters are decoupled to produce free water molecules (*free* state). This model was successfully applied by Labrador-Paez et al. to explain the anomalous thermal properties in the luminescence of Eu^{3+} aqueous complexes[12] and nanocrystals in water,[13] while Brites et al. moved within this framework to describe the crossover temperature observed in the Brownian velocity of colloidal upconverting nanoparticles in water.[9] In this sense, the

D. H. Ortgies, A. Benayas, D. Jaque, E. Martín Rodríguez, J. García Solé
Nanomaterials for Bioimaging Group (nanoBIG)
Instituto Ramón y Cajal de Investigación
Sanitaria (IRICYS)
Hospital Ramón y Cajal
Ctra. De Colmenar Viejo km 9.100, Madrid 28034, Spain
F. E. Maturi, L. D. Carlos
Phantom-g
CICECO -Aveiro Institute of Materials
Department of Physics
University of Aveiro
Aveiro 3810-193, Portugal

changes in the absorption spectrum of water at different temperatures must be due to the coexistence of both states.

In this paper, we have carried out a systematic analysis of the liquid water absorption spectrum in the biological windows (750–1800 nm) within the 25–65 °C range—a temperature range that encompasses the physiological range (25–50 °C). The main absorption bands have been explained as the convolution of two Gaussian components, each of them corresponding to one of the two above-mentioned states of liquid water. Despite its simplicity, this approach reasonably explains the temperature dependence of the shape of the absorption bands experimentally observed.

From a practical standpoint, the absorption of liquid water can seriously affect the emission spectral shape of nanoparticles in aqueous colloidal dispersions, therefore reducing their reliability for thermal sensing when used as luminescent nanothermometers in biological and/or biomedical applications.[14] Among the proposed nanothermometers, those based on biocompatible Ag_2S nanoparticles (NPs) are the best-performing ones.[15] Their performance is related to their high brightness (the product between absorption cross-section and emission efficiency) in the NIR-II window (1000–1350 nm) and the large sensitivity of different emission features to slight temperature variations within the physiological temperature range. Thus, the second part of this work is dedicated to the evaluation of the effect of water absorption on the emission shape of Ag_2S NPs and how the temperature variation of the absorption bands of water affects the thermometric properties of these nanoparticles.

2. Background: Water Molecule Vibrations and Their Near-Infrared Absorption

Water molecules display three normal vibrational modes that involve symmetric stretching (mode I), symmetric bending (mode II), and asymmetric stretching (mode III) of the covalent bonds. They can be properly described by the three corresponding vibrational quantum numbers ν_1 (mode I), ν_2 (mode II), and ν_3 (mode III). In the ground state, these quantum numbers are all equal to 0, so the ground state can be labeled as (0, 0, 0). The fundamental vibrational transitions of a water molecule correspond to transitions in which only one of the three vibrational quantum numbers changes by one unit. Thus, following the selection rule $\Delta\nu_i = 1$, these transition bands are usually written as[16]

Mode I: (0, 0, 0) → (1, 0, 0);
Mode II: (0, 0, 0) → (0, 1, 0);
Mode III: (0, 0, 0) → (0, 0, 1).

For individual molecules (*free* state), these absorption fundamental transitions lie at 2.73 µm (mode I), 6.27 µm (mode II), and 2.66 µm (mode III), and thus, spectrally far away from the biological windows. Nevertheless, due to anharmonicity, further transitions are allowed from the ground state (0, 0, 0) to higher states with $\Delta\nu_i > 1$ (overtones) and even to excited states with a simultaneous change of more than one vibrational quantum number, i.e., transitions from the (0,0,0) fundamental state to a (ν_1, ν_2, ν_3) excited state, upon absorption of a single photon. In the latter, typically called combination transitions, the excited state is a mixture of the three vibrational modes.

The previously mentioned transitions have been used to describe the absorption spectrum of water in the vapor state,[16] as it is the closest situation to free water molecules. However, compared to the vapor state, the absorption bands of liquid water are noticeably broader, the peaks are usually shifted and they may exhibit several new features. This is partially due to intermolecular vibrations (collective excitation of several molecules) giving rise to a whole new array of vibrational states of the molecule for the same vibrational quantum numbers.[17] Nevertheless, the main features of the liquid water absorption resemble somehow the ones from individual molecules and hence those observed in the vapor phase.[16] Despite the main absorption bands of liquid water have been well labeled in terms of transitions using the quantum numbers of single molecules, the general recognition that liquid water displays two states[7] produces a more complex structure of its absorption spectrum with respect to the one exhibited by water molecules in the vapor state. Thus, in a first approach, this structure could be described via the superposition of the spectra of these two states. As a matter of fact, a two-state outer-neighbor bonding model already provided a good microscopic explanation for the temperature dependence of pure liquid water's absorption in the visible-NIR (550–900 nm) spectral region.[6c]

3. Experimental Results and Discussion

3.1. Absorption of Liquid Water in the Biological Windows

First, since the scattering of water compared to its absorption is very small, we have considered that it can be neglected, and so the term absorption is herein used as a synonym for extinction in water. **Figure 2** shows the room temperature (25 °C) absorption coefficient (α) spectrum of ultrapure water (pH = 7) in the wavelength range 800–1700 nm, i.e., in the spectral range of interest for deep-tissue biomedical applications. The well-known biological windows NIR-I (750–950 nm), NIR-II (1000–1350 nm), and NIR-III (1500–1800 nm) have also been indicated in this figure. The spectrum consists of three main overlapping bands whose intensity increases at longer wavelengths. These bands, roughly centered at 1000, 1200, and 1450 nm, have been labeled as bands I, II, and III, respectively. It can be noted that band I arises in the boundary between NIR-I and NIR-II, band II falls within NIR-II, and band III demarcates the end of NIR-II and the beginning of NIR-III. It is also important to mention that previously reported bands peaking at 836 and 888 nm[5c,6c] are too weak and hence negligible compared to the main bands I, II, and III.

According to previous review works,[16] these bands can be mostly assigned to vibrational combination transitions (see Section 2). The dominant absorption band III should be assigned to the vibrational combination transitions (0, 0, 0) → (a, 0, b), a and b being integer numbers in which; $a + b = 2$. The weaker absorption bands are associated with transitions (0, 0, 0) → (a, 1, b); with $a + b = 2$ (band II), and (0, 0, 0) → (a, 0, b); with $a + b = 3$ (band I). A careful inspection of the shape

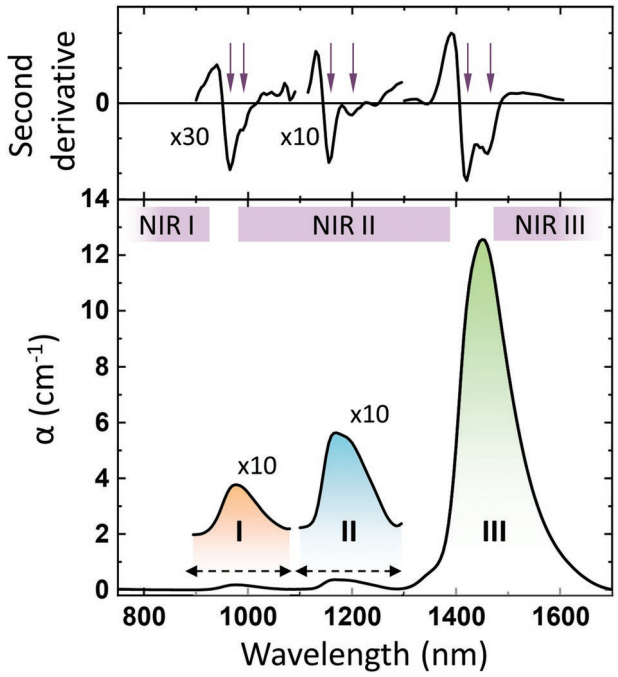

Figure 2. Bottom: Absorption coefficient (α) spectrum of liquid water at room temperature. The three main absorption bands are denoted in different colors and labeled I, II, and III, respectively. NIR-I, NIR-II, and NIR-III biological windows are also displayed. Top: Second derivative of α. The two minima of each peak are indicated by arrows.

of these bands reveals that they are not single absorption bands but consist of more than one component. This observation is supported by the shape of the second derivative of the absorption spectrum (see the top part of Figure 2). Each band is composed of at least two main components (two minima in the corresponding second derivative spectrum) peaking at 965 and 990 nm (band I), 1155 and 1195 nm (band II), and 1415 and 1460 nm (band III). Importantly, the high-energy component of each band is closer to the main peaks reported for water molecules in the vapor state (940 nm (band I), 1130 nm (band II), and 1380 nm (band III)) than the low energy components.[16]

3.2. Temperature Dependence of the Absorption Bands

The absorption spectrum of liquid water (and its second derivative) was systematically recorded as a function of temperature in the range 25–65 °C, with temperature steps of 5 °C (see Figure S1 in the Supporting Information). **Figure 3**a shows the absorption spectra taken at different temperatures for each band separately. This figure reveals that both the shape and the maximum values of the absorption coefficient (α_{max}) of each band are affected by temperature changes. In general, α_{max} of each band is slightly increased (Figure 3b) and blue-shifted (Figure 3c) as the temperature increases, in good agreement with previous results.[5c,6e,6f,6h] More precisely, α_{max} of bands I and II increase by about 11% and 22%, respectively, while α_{max} of band III only increases by about 1.5%, The blue-shifts observed in these bands are about 5 nm (53 cm^{-1}, band I), 5 nm (37 cm^{-1}, band II), and 20 nm (97 cm^{-1}, band III). An important aspect is that signatures of a bilinear behavior appear in the temperature-induced blue-shift trends (peak position vs temperature, Figure 3c) of bands I and III, showing a crossover temperature at around 45 °C. Bilinear behaviors have been previously observed in many physical properties of liquid water.[11] These behaviors have indeed been related to the coexistence of the two different states (*free* and *ice*) of water molecules in the liquid phase, whose relative concentration changes with temperature and produces a crossover temperature between 40 and 50 °C,[9,11,12] depending on the pH of the medium.[12]

To interpret the results given in Figure 3, we assumed the simple two-states approach of liquid water described in the Introduction Section, therefore, each absorption band was fitted by the convolution of two Gaussian components. Within this model, the two components of each band should correspond to the two above-mentioned states of liquid water. **Figure 4**a shows the best fit obtained for the three NIR absorption bands at room temperature (25 °C). All the absorption bands are reasonably fitted (r^2 varying between 0.982 and 0.993) by the convolution of two bands, labeled as *ice* and *free* with the *ice* bands peaking at longer wavelengths than the *free* ones. We could now establish that the dominant bands at lower temperatures should be related to the *ice* state, while the weak bands should be related to the *free* state, i.e., to the small number of free molecules coexisting with the *ice* molecules at 25 °C.

The next step was the evaluation of the evolution of the *ice* and *free* components of the three absorption bands upon heating. For this purpose, the two-band convolution was obtained at each temperature. It is important to point out that the peak positions (λ_{max}) of the *ice* and *free* components were obtained from the corresponding position of the second derivative minima at a given temperature (see Figure S1, Supporting Information) and optimized during the middle step of the fitting procedure, so they are not varying parameters as described in the Experimental Section. Thus, in the last step of the fitting process, the only free parameter is the value of α_{max} of the *ice* and *free* components that should be related to the relative concentration of molecules in the *ice* and *free* state at each temperature.

Figure 4b shows that as temperature rises, the net absorption of *free* bands increases while the one corresponding to the *ice* bands decreases. In other words, a temperature increase produces an increase in the concentration of *free* state molecules and a simultaneous decrease in the concentration of molecules in the *ice* state. As shown in the upper insets of Figure 4b, this approach reasonably explains (within a 4% of uncertainty) the experimental results given in Figure 3b. In addition, this two-Gaussian fit explains (within a 0.3% accuracy) the blue-shift experimentally observed as the temperature is raised. Therefore, by this simple approach, the blue-shift and maximum absorption value variations induced by temperature changes can be reasonably explained by the increase in the concentration of molecules in the *free* state at the cost of a decrease in the concentration of molecules in the *ice* state. Thus, the main temperature-induced shape changes in the absorption bands of liquid water can be convincingly explained because of the

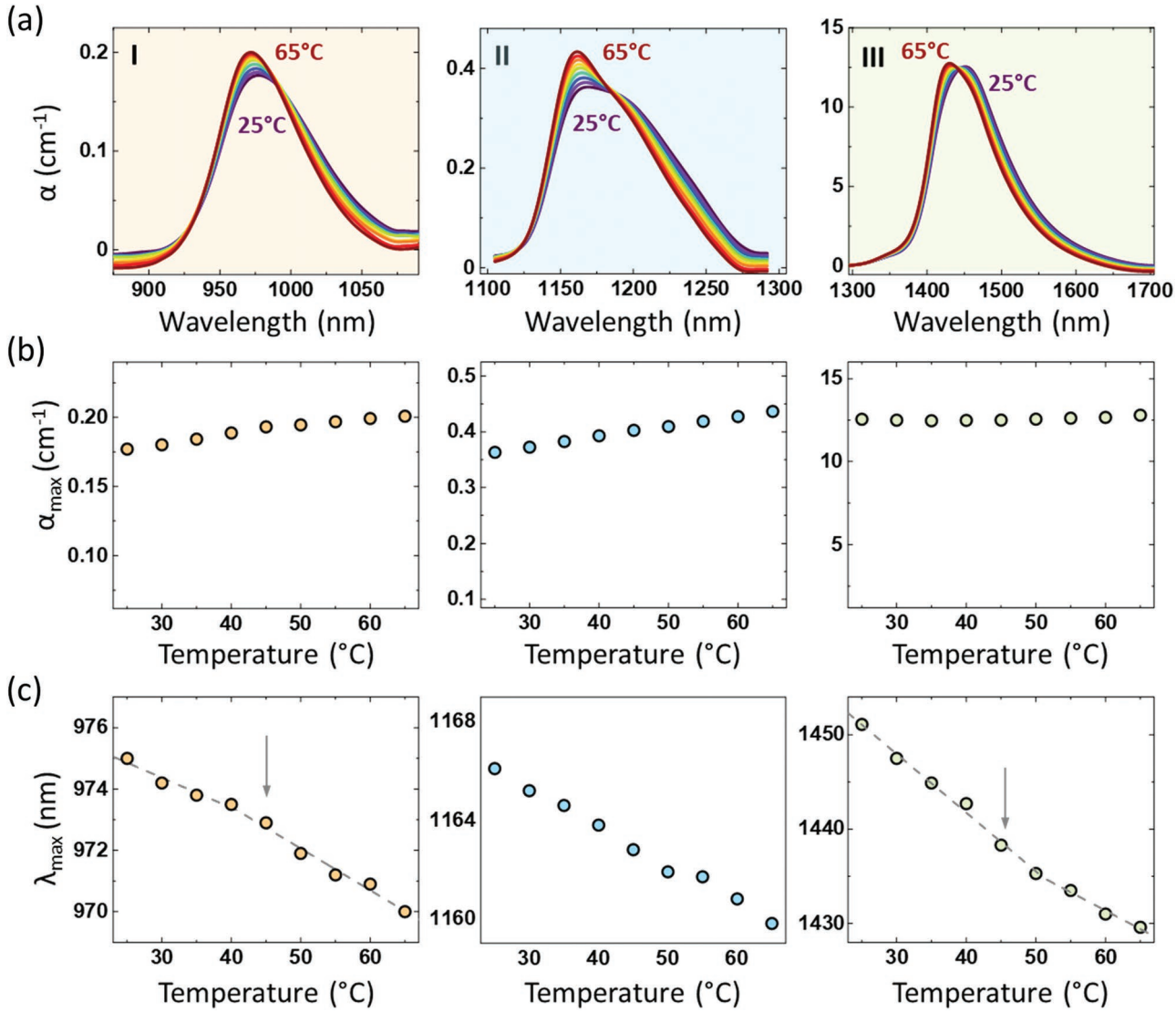

Figure 3. a) Temperature dependence of the I, II, and III absorption bands in the temperature range from 25 to 65 °C. Each band is represented after subtracting the corresponding background. b) Maximum value of the absorption coefficient (α_{max}) of each band as a function of temperature. c) Peak position (λ_{max}) of the bands as a function of temperature. The results for bands I and II have been fitted into a bilinear behavior. Arrows indicate the temperature in which the change of slope takes place.

disaggregation of small water clusters (*ice* state) into free molecules (*free* state) as the temperature increases.

3.3. Effects on Luminescent Nanothermometers

To study the temperature effect of water absorption in an aqueous dispersion of nanoparticles, we have investigated the behavior of Ag_2S nanoparticles (NPs) used as luminescent nanothermometers. Thus, Ag_2S NPs are an excellent case study to examine the effect of water absorption on the spectral shape of NIR-emitting nanoparticles. In that vein, first, the effect of water absorption at room temperature on the emission shape of the Ag_2S NPs was investigated (Section 3.3.1). Second, the study of how these temperature-dependent absorption effects can affect the thermometric properties in the physiological temperature range was performed (Section 3.3.2).

3.3.1. Effect of Water Absorption on the Ag_2S Nanoparticles Emission Spectral Shape

To investigate the effect of water absorption on the emission spectral shape of the Ag_2S nanoparticles, the emission spectrum as a function of the depth in the dispersion was measured, as schematized in **Figure 5**a (for further details of the setup, see the Supporting Information and Figure S2). Briefly, a fixed volume of the Ag_2S NPs/water dispersion (active volume) was excited while recording the room temperature emission spectrum after traveling through different depths h in the dispersion

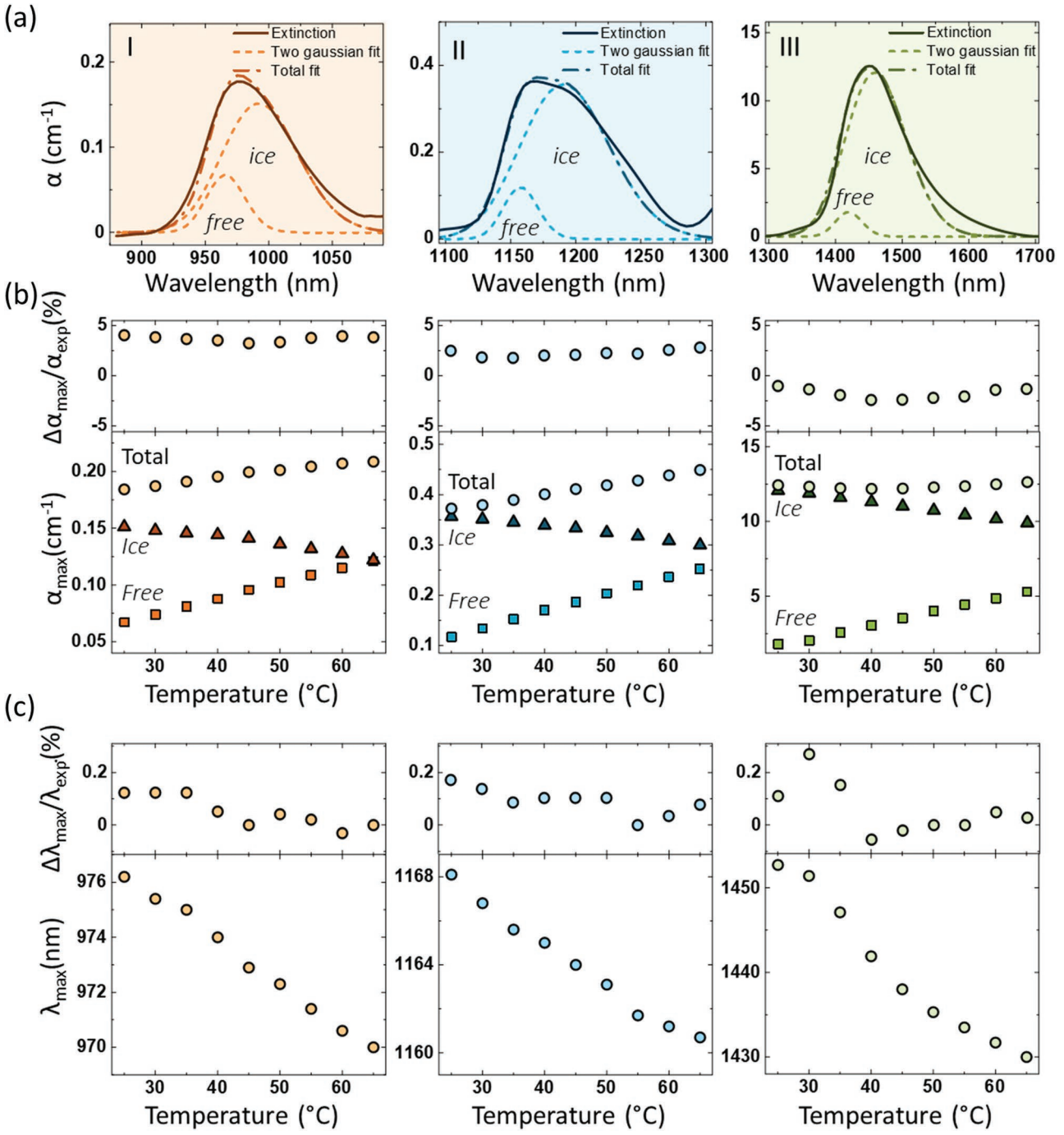

Figure 4. a) Gaussian convolution of the absorption bands at 25 °C. b) Bottom: Temperature evolution of the fitted maximum absorption coefficient (α_{max}) of the two components (*ice* and *free*) and the resulting sum (total). Top: relative error between the fitted α_{max} and the experimental one (α_{exp}). c) Bottom: Peak position (λ_{max}) versus temperature for the I, II, and III bands as obtained by the two Gaussian fits. Top: relative error between the fitted and the experimental peak position (λ_{max}).

(nonactive volume), given by the exceeding volume. The morphological and optical characterization of the Ag_2S NPs used in this work is given in Figure S3 in the Supporting Information.

Figure 5b shows that the emission spectral shape of the nanoparticles is drastically affected as h is increased. In particular, the long-wavelength side of the spectrum (1150–1350 nm) is strongly reduced when h increases and the emitted light pathway in the surrounding medium is increased. To explain this effect, we now consider how the NIR radiation emitted by the Ag_2S nanoparticles is attenuated when traveling along with the surrounding medium. This attenuation is given by the Beer–Lambert law. According to this law, the emission intensity

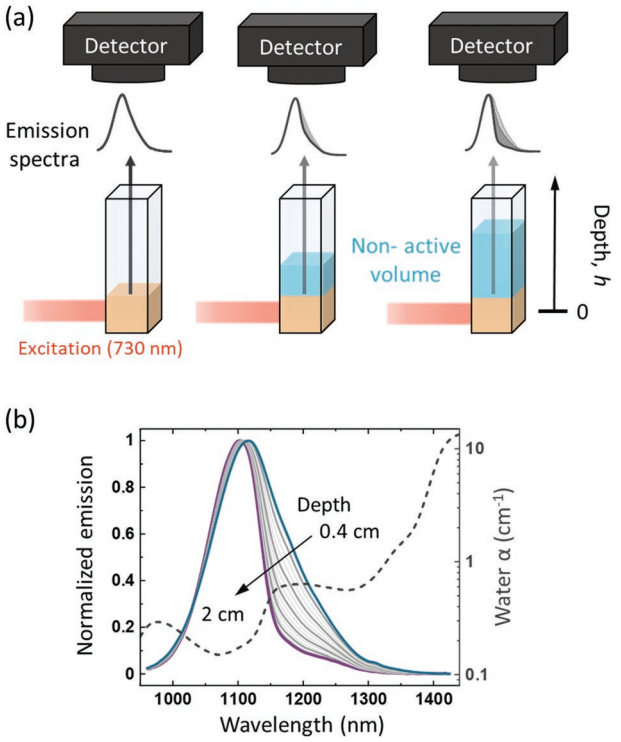

Figure 5. a) Schematic representation of the experiment performed to evaluate the effect of the depth in the dispersion on the emission of the Ag_sS NPs. b) Normalized emission spectrum of the Ag_sS NPs aqueous dispersion at 25 °C as a function of the excitation depth in the cuvette. Absorption coefficient (α) of water in the same spectral region is plotted (see dotted line) to demonstrate that the emission changes are due to water absorption.

reaching the detector, $I(\lambda,h)$, decreases exponentially with the source depth as

$$I(\lambda,h) \sim I_0(\lambda) e^{-h^* \alpha_{ext}(\lambda)} \quad (1)$$

where $I_0(\lambda)$ is the emitted intensity from the active volume, λ is the wavelength of the emitted photons, $\alpha_{ext}(\lambda)$ is the extinction coefficient, and h^* is the average distance traveled by the emitted photons—which depends on h and the number of internal reflections of the emitted photons in the cuvette wall before reaching the detector, h^* being always larger than h. Extinction of emitted light can be due to both absorption and scattering, therefore

$$\alpha(\lambda) = \alpha_{abs}(\lambda) + \alpha_{scat}(\lambda) \quad (2)$$

where $\alpha_{abs}(\lambda)$ and $\alpha_{scat}(\lambda)$ are the absorption and scattering coefficients, respectively. However, in the present study, the scattering effect can be neglected as the scattering centers (nanoparticles) are three orders of magnitude smaller than the analyzed wavelengths. Thus, $\alpha_{ext}(\lambda) \simeq \alpha_{abs}(\lambda)$, and Equation (1) can be written as

$$I(\lambda,h) \sim I_0(\lambda) e^{-h^* \alpha_{abs}(\lambda)} \quad (3)$$

In addition, the absorption of the Ag_2S NPs dispersion at the spectral range of their emission (1000–1300 nm) is very small (see Figures S3 and S7, Supporting Information) even at high concentrations (up to 1 mg mL^{-1}), so we can consider that the absorption coefficient $\alpha_{abs}(\lambda)$ is just that of water.

The absorption spectrum of liquid water (dotted line) in the emission range of the Ag_2S NPs was included in Figure 5b. It is important to point out that the band around 1200 nm (band II in Figure 2) overlaps with the long-wavelength side of the Ag_2S NPs emission spectrum, and so this part of the emission will be more absorbed than the short-wavelength side. Indeed, Figure S4 in the Supporting Information shows that the emitted light at 1200 nm (i.e., the long-wavelength emission side) decreases exponentially with h. This behavior is satisfactorily explained by Equation (3) with $\alpha_{abs}(\lambda) \approx 0.33$ cm^{-1} (the absorption coefficient of liquid water) and an average path of about $h^* = 3h$ (see Section S4 in the Supporting Information), as the emitted light travels an average path larger than the straight path of length h. In fact, this behavior is not observed when the Ag_2S nanoparticles are dispersed in heavy water (D_2O), whose absorption coefficient at this wavelength (0.02 cm^{-1}) is negligible compared to that of water (see Figure S5, Supporting Information). Consequently, the shape modifications in the emission spectrum of the Ag_2S NPs aqueous dispersion as h increases are undoubtedly due to wavelength-dependent water absorption of the photons emitted by the Ag_2S nanoparticles. This result is also supported by the fact that Ag2S NPs do not reabsorb the signal in such spectral range around 1200 nm (see Section S7 in the Supporting Information).

3.3.2. Effect of Water Absorption on Ag_2S Nanothermometric Properties

As previously discussed (Section 3.2), the absorption coefficients of water in the NIR are clearly temperature-dependent. Thus, water absorption effects are expected to have a sizable impact when Ag_2S nanoparticles dispersed in water are used as nanothermometers. Temperature sensing using these NPs is based on the temperature dependence of different emission features. Among those ones, emission intensity, peak position, and the ratio between the intensity at two wavelengths are generally used.[18] Recently, the luminescence lifetime of Ag_2S NPs has been also proposed as a reliable thermometric parameter to overcome the problems related to tissue absorption and scattering.[19] To highlight the importance of the effect of water absorption, we have carried out a comparative study of the temperature-dependent emission of Ag_2S nanoparticles dispersed in H_2O and D_2O.

Figure 6a shows the emission spectra of Ag_2S NPs dispersed in the two solvents at different temperatures. In both dispersions, the emission intensity decreases upon heating. This decrease is mostly due to thermal quenching of the Ag_2S luminescence, because, once the exciton Bohr radius of Ag_2S is 2.2 nm,[20] the luminescence properties of the obtained nanoparticles (3 nm in radius) are not dominated by quantum effects.[20] Regardless of the quenching mechanism, it is important to note that the dispersion in water heavily affects the emission shape of the NPs while it remains almost unaffected when

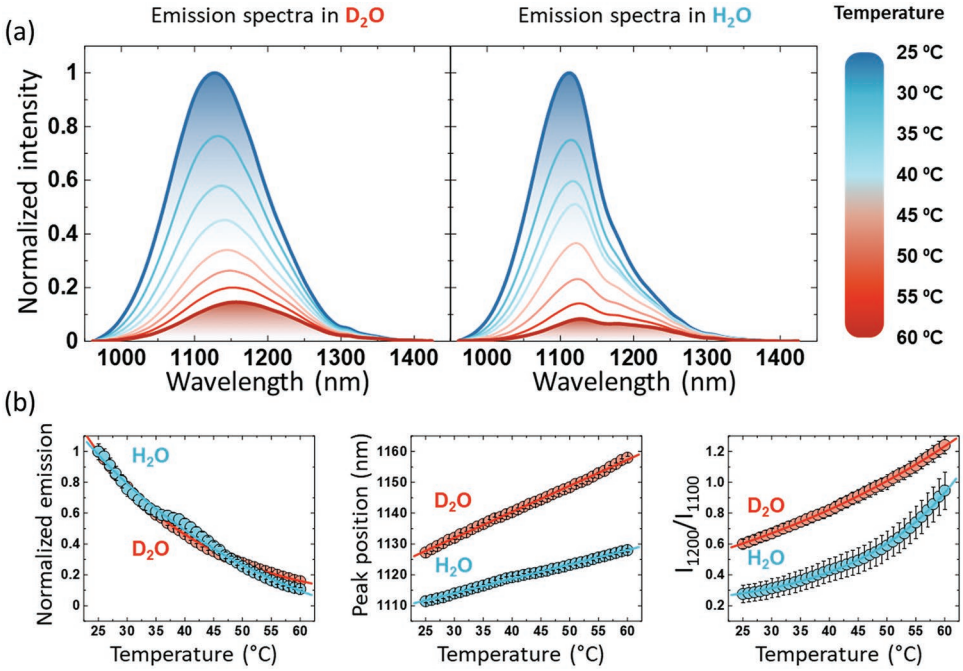

Figure 6. a) Normalized emission spectra of Ag_2S NPs dispersed in heavy water and water at different temperatures. b) Temperature dependence of the different thermometric parameters defined for the Ag_2S NPs dispersed in water (blue) and heavy water (red): normalized total emission intensity (left), peak position (center), and intensity ratio (right). The solid lines are guides for the eyes.

dispersed in heavy water. This occurs because the absorption is significantly smaller in D_2O than in H_2O in the emission range of the Ag_2S NPs (1000–1300 nm, Figure S5, Supporting Information). Additionally, the temperature increase induces a redshift in the emission of the Ag_2S NPs dispersed in heavy water and water, which is related to the temperature dependence of the energy bandgap of Ag_2S.[21]

To investigate how water affects the thermometric parameters of the Ag_2S NPs, Figure 6b reports the temperature dependence of the normalized total emitted intensity (I), peak position, and the intensity ratio between the intensities at 1200 nm (I_{1200}) and 1100 nm (I_{1100}) for the Ag_2S nanoparticles in both dispersion media. While the total intensity in heavy water presents a monotonous decrease with increasing temperature, this decrease is discontinuous for the nanoparticles in water, displaying an anomalous increase around 40–45 °C, just where a water dielectric anomaly takes place.[11a,12] The influence of reabsorption is more dramatic when considering the redshift of the emission peak as the thermometric parameter. As the temperature increases from 25 to 60 °C, the emission redshifts 132 cm^{-1} for the nanoparticles dispersed in H_2O while the redshift is 235 cm^{-1} for the D_2O dispersion. Consequently, a smaller redshift is observed for the Ag_2S nanoparticles dispersed in water because water presents high optical absorption in the same spectral region in which the luminescence of the Ag_2S NPs takes place.

The ratiometric parameter also displays a quite different temperature dependence when comparing the results obtained in D_2O and H_2O, as shown in the corresponding part of Figure 6b. While for the dispersion in heavy water this trend is almost linear, a bilinear trend is observed for the dispersion in water, with a crossover temperature around 45 °C. This is again a signature of the influence of water absorption in the thermometric properties of the aqueous dispersion of Ag_2S nanoparticles.

The impact of the absorption of water on the thermometric parameters of Ag_2S can be further assessed through the evaluation of the thermometric performance of the Ag_2S NPs dispersed in D_2O and H_2O. The performance of a luminescent thermometer is usually evaluated by its relative thermal sensitivity $\left(S_r = \frac{1}{\Delta}\left|\frac{\partial\Delta}{\partial T}\right|\right)$, which is the change in the thermometric parameter (temperature-dependent optical property, usually denoted by Δ) per degree of temperature change, and the uncertainty in temperature $\left(\delta T = \frac{1}{S_r}\frac{\delta\Delta}{\Delta}\right)$, corresponding to the smallest temperature resolvable by the thermometer.[22] The maximum relative thermal sensitivity (S_m) and minimum δT obtained for the different thermometric parameters of the Ag_2S NPs are reported in **Table 1** (see Section S6 of the Supporting Information for a detailed description of the calculation of S_r and δT).

The results in Table 1 demonstrate that the S_m of the total emission intensity (I) and the intensity ratio (I_{1200}/I_{1100}) approaches are higher in H_2O, because the reabsorption by water results in a noticeable change in the emission profile of the Ag_2S NPs, thus producing a wider shift of Δ upon heating. Nevertheless, the relative uncertainty of S_m ($\delta S_m/S_m$) is increased in water, which explains the increase of δT when moving the Ag_2S NPs from heavy water to water. This is a side effect of the reabsorption of water, which reduces the signal-to-noise ratio of the emission spectra, causing the relative

Table 1. Maximum relative thermal sensitivity (S_m), uncertainty in S_m (δS_m), minimum uncertainty in temperature (δT), uncertainty in δT ($\sigma_{\delta T}$), and temperature at which they occur (T_m) for the different thermometric parameters of the Ag_2S nanoparticles dispersed in heavy water and water.

Δ	Heavy water			Water		
	$S_m \pm \delta S_m$ [% °C^{-1}]	$\delta T \pm \sigma_{\delta T}$ [°C]	T_m [°C]	$S_m \pm \delta S_m$ [% °C^{-1}]	$\delta T \pm \sigma_{\delta T}$ [°C]	T_m [°C]
peak position	$(7.48 \pm 0.05) \times 10^{-2}$	0.53 ± 0.01	25	$(4.19 \pm 0.04) \times 10^{-2}$	0.95 ± 0.01	25
I	5.43 ± 0.21	0.44 ± 0.02	60	14.88 ± 1.51	0.42 ± 0.05	60
I_{1200}/I_{1100}	2.09 ± 0.17	2.22 ± 0.21	25	4.65 ± 1.05	3.66 ± 1.03	60

uncertainty of the thermometric parameter ($\delta\Delta/\Delta$) to increase, consequently increasing the uncertainty of the temperature readout in water. These results indicate that despite Ag_2S being the best nanothermometers used for thermal sensing in vivo applications,[23] their thermometric performance is heavily affected by the absorption arising from water, resulting in lower accuracy and reproducibility, which are major drawbacks when performing thermal readouts. Since all the emission features (peak position, redshift, and intensity ratio at two different wavelengths) are affected by the temperature dependence of water absorption, this factor must be carefully considered when using Ag_2S dispersed in water and aqueous media as nanothermometers.

4. Conclusion

In this work, we have systematically analyzed the absorption spectrum of ultrapure water with pH = 7 in the biological spectral windows (750–1800 nm) as a function of temperature in the extended physiological range 25–65 °C. The spectrum consists of three main absorption bands that increase and blue-shift as the temperature is raised. This behavior can be reasonably explained in terms of a two-state model for the water molecules in liquid water. Then we have demonstrated that temperature-induced changes in liquid water absorption have a relevant effect on the performance of Ag_2S luminescent nanothermometers, the most efficient and sensitive nanothermometers reported to date. All the spectral thermometric parameters (emission intensity, peak shift, and intensity ratio) are severely affected due to the water absorption of the Ag_2S nanoparticles emission, demonstrating the need for further standardization in order to achieve improved reproducibility and reliability for nanothermometry applications in aqueous media.

5. Experimental Section

Temperature Dependence of Water Absorption Spectra: The absorption spectra of ultrapure water obtained from a Milli-Q equipment were measured with a double-beam absorption spectrometer (Lambda1050, Perkin Elmer) with a spectral resolution of 5 nm and using a quartz cuvette with 2 mm path length. To investigate the evolution of the water absorption spectrum with temperature, a Peltier temperature controller (Q-pod 2e, Quantum Northwest) was placed inside the spectrometer enabling the selection of the desired temperature. Measurements were taken every 5 °C after 5 min of thermal stabilization in the 25–65 °C range.

Spectral Fitting of Liquid Water Absorption Bands: The NIR absorption spectra were fitted following a three-step approach using a MATLAB (version R2019b) custom code. In the first step, a background signal was defined and used to correct all the spectra. To define the background, the absorption spectrum of water at room temperature was plotted in Origin (version 2017) and the Create Baseline tool with the Second Derivative Method was used. In the second step, the three main absorption bands (see Figure 2) were adjusted to two Gaussian functions. For these fittings, the peak position of each component was set and fixed to the peak wavelengths obtained from the second derivative spectra (see Figure 2 and Figure S1, Supporting Information), while leaving the full-widths at half-maximum and peak heights (maximum value of the absorption coefficients) as free parameters. In the third step, the full-widths at half-maximum were fixed to the mean value for the different temperatures, and both the fixed width and peak position were slightly changed in each iteration until the optimal fitting (the one minimizing the r^2 values) was achieved.

Ag_2S Nanoparticles Dispersions: Silver nitrate ($AgNO_3$), sodium sulfide ($Na_2S{\cdot}9H_2O$), 11-mercaptoundecanoic acid (11-MUA), and ammonia (NH_3) were obtained from Sigma Aldrich and used as received. The Ag_2S nanoparticles were synthesized as follows: 273 mg of 11-MUA were dissolved in 38 mL of water, then 42.5 mg of $AgNO_3$ dissolved in 1.0 mL of water were added. The pH was adjusted to 8 with ammonia. The solution was stirred for 24 h, protected from light. After that time, 30 mg of $Na_2S{\cdot}9H_2O$ dissolved in 11 mL of water was added to the solution. Subsequently, the reaction was transferred to a monomodal microwave cavity and heated up to 100 °C (300 W) for 5 min under magnetic stirring, following the procedures reported elsewhere.[24] After this short microwave heating program, Ag_2S nanoparticles decorated with 11-MUA were washed with absolute ethanol.

Emission Spectra of Ag_2S Nanoparticles Dispersions in Various Media: The emission spectra of Ag_2S NPs dispersions in water and heavy water (both with a concentration of 0.2 mg mL^{-1}) were recorded using the experimental setup described in Figure S2 of the Supporting Information. To evaluate the water-induced changes in the shape of the emission band of the Ag_2S, two different experiments were performed. First, the emission spectra of Ag_2S NPs dispersed in water for different depths (Figure 5) were recorded using an infrared hyperspectral camera (PyLoN-IR, Princeton). The 730 nm excitation beam was collimated with a 5 cm focal collimator to excite the area closest to the dispersion/air interface (see inset of Figure S2, Supporting Information). Then, the dispersion volume was progressively increased from 1.0 to 2.6 mL by adding sequentially 0.1 mL of dispersion.

According to this experimental arrangement, each Ag_2S nanoparticle located inside the illuminated volume behaved as an emitting source of IR light. Due to the nonneglectable spot size, the depth was considered to be starting at the center of the beam, and so, the shortest depth that could be measured was 0.4 cm (when using a volume of 1.0 mL of the sample). For dispersions having a volume higher than 1.0 mL, a certain volume of the sample (denoted as exceeding volume) was located outside the light-emitting diode excitation area. Ag_2S nanoparticles located outside the excitation area were not photoactivated, so they did not emit any photons. Indeed, when the volume of the dispersion of Ag_2S nanoparticles was increased above 1.0 mL, the nonactive volume behaved like a filter placed between the emitting Ag_2S NPs and the detector. Thus, before reaching the detector, the incident emission coming from Ag_2S sources ($i_0(\lambda, T)$) went through the filter-like medium, where photons could be absorbed or scattered. Consequently, the higher

Particle & Particle Systems Characterization
www.particle-journal.com

the sample volume, the higher the exceeding volume, and so the larger signal depth in the medium.

The second set of experiments was devoted to the analysis of how the changes in the absorption of water due to temperature differences affect the shape of the emission bands of the Ag_2S NPs. The emission spectra were measured at one fixed depth (h = 1.6 mm) and the temperature was varied in 1.0 °C steps (Figure 6). This experiment was done with the NPs dispersed in water and heavy water to compare the effects of water with those of a nonabsorbing solvent in that spectral range. The processing of the temperature-dependent emission spectra of the Ag_2S NPs dispersed in D_2O and H_2O was performed by using a custom script written in MATLAB (version R2019b) where a polynomial baseline correction was applied to remove the electrical noise from the hyperspectral camera and the obtained spectra were normalized by the maximum intensity of the emission at 25.0 °C for each medium (i.e., heavy water and water) afterward.

Nanothermometry on Ag_2S Nanoparticles: To assess the thermal sensing capability of the obtained nanoparticles in D_2O and H_2O, three distinct thermometric parameters were obtained from the temperature-dependent emission spectra of the Ag_2S NPs. The total emitted intensity was computed as the integrated emission between 960 and 1425 nm (the integrated intensities were normalized by dividing the obtained integrated areas by the integrated area at 25.0 °C for comparison purposes) and its corresponding uncertainty (error bar) was the total integrated intensity multiplied by the inverse signal-to-noise ratio. The peak position was obtained by adjusting a parabola to the emission spectra considering values between 95% and 100% of the maximum intensity from each spectrum and the uncertainty was the spectral resolution (wavelength increment) of the hyperspectral camera. The intensity ratio was the ratio between the intensities at 1200 nm (I_{1200}) and 1100 nm (I_{1100}) for the Ag_2S NPs in both media with the uncertainty corresponding to the propagation of uncertainties from the intensity ratio I_{1200}/I_{1100}.

Supporting Information

Supporting Information is available from the Wiley Online Library or from the author.

Acknowledgements

This work was financed by the Spanish Ministerio de Ciencia e Innovación under project PID2019-106211RB-I00, by the Instituto de Salud Carlos III (PI19/00565), by the Comunidad Autónoma de Madrid (S2017/BMD3867 RENIM-CM) and co-financed by the European structural and investment fund. Additional funding was provided by the European Union Horizon 2020 FETOpen project NanoTBTech (801305), the Fundación para la Investigación Biomédica del Hospital Universitario Ramón y Cajal project IMP21_A4 (2021/0427), and by COST action CA17140. A.B. acknowledges funding support through the TALENTO 2019T1/IND14014 contract (Comunidad Autónoma de Madrid). F.E.M. and L.D.C. acknowledge the financial support received from the project Shape of Water (PTDC/NAN-PRO/3881/2020) through Portuguese funds.

Conflict of Interest

The authors declare no conflict of interest.

Data Availability Statement

The data that support the findings of this study are available from the corresponding author upon reasonable request.

Keywords

nanothermometry, silver sulfide, temperature dependence, water absorption

Received: May 18, 2022
Revised: July 9, 2022
Published online: September 14, 2022

[1] J. R. Collins, *Phys. Rev.* **1925**, *26*, 771.
[2] W. C. Röntgen, *Ann. Phys.* **1892**, *281*, 91.
[3] a) C. K. N. Patel, A. C. Tam, *Nature* **1979**, *280*, 302; b) E. H. Otal, F. A. Iñón, F. J. Andrade, *Appl. Spectrosc.* **2003**, *57*, 661; c) E. D. Jansen, T. G. van Leeuwen, M. Motamedi, C. Borst, A. J. Welch, *Lasers Surg. Med.* **1994**, *14*, 258; d) V. V. Semak, A. Gerakis, M. N. Shneider, *AIP Adv.* **2019**, *9*, 085016; e) D. Theisen-Kunde, V. Danicke, M. Wendt, R. Brinkmann, in *4th European Conf. Int. Federation for Medical and Biological Engineering* (Eds: J. Vander Sloten, P. Verdonck, M. Nyssen, J. Haueisen), Springer, Berlin, Heidelberg **2009**, pp. 2228–2229; f) W. S. Pegau, J. R. V. Zaneveld, *Limnol. Oceanogr.* **1993**, *38*, 188.
[4] a) E. Hemmer, A. Benayas, F. Légaré, F. Vetrone, *Nanoscale Horiz.* **2016**, *1*, 168; b) A. M. Smith, M. C. Mancini, S. Nie, *Nat. Nanotechnol.* **2009**, *4*, 710.
[5] a) L. Sordillo, Y. Pu, S. Pratavieira, Y. Budansky, R. Alfano, *J. Biomed. Opt.* **2014**, *19*, 056004; b) J. A. Curcio, C. C. Petty, *J. Opt. Soc. Am.* **1951**, *41*, 302; c) V. Hollis, T. Binzoni, D. Delpy, *Proc. SPIE* **2001**, *4250*, 434506.
[6] a) S. H. Chung, A. E. Cerussi, S. I. Merritt, J. Ruth, B. J. Tromberg, *Phys. Med. Biol.* **2010**, *55*, 3753; b) J. B. Cumming, *Nucl. Instrum. Methods Phys. Res., Sect. A* **2013**, *713*, 1; c) V. S. Langford, A. J. McKinley, T. I. Quickenden, *J. Phys. Chem. A* **2001**, *105*, 8916; d) L. Kou, D. Labrie, P. Chylek, *Appl. Opt.* **1993**, *32*, 3531; e) N. Kakuta, A. Ozaki, F. Li, H. Arimoto, Y. Yamada, in *29th Annual Int. Conf. IEEE Engineering in Medicine and Biology Society*, IEEE, Piscataway, NJ **2007**, pp. 4564–4567; f) N. Kakuta, F. Li, Y. Yamada, in *Conf. Proc. IEEE Engineering in Medicine and Biology Society*, IEEE, Piscataway, NJ **2005**, pp. 3145–3148; g) N. Kakuta, H. Arimoto, H. Momoki, F. Li, Y. Yamada, *Appl. Opt.* **2008**, *47*, 2227; h) N. Kakuta, K. Kondo, A. Ozaki, H. Arimoto, Y. Yamada, *Int. J. Heat Mass Transfer* **2009**, *52*, 4221.
[7] a) P. Gallo, K. Amann-Winkel, C. A. Angell, M. A. Anisimov, F. Caupin, C. Chakravarty, E. Lascaris, T. Loerting, A. Z. Panagiotopoulos, J. Russo, J. A. Sellberg, H. E. Stanley, H. Tanaka, C. Vega, L. Xu, L. G. M. Pettersson, *Chem. Rev.* **2016**, *116*, 7463; b) J. R. Errington, P. G. Debenedetti, *Nature* **2001**, *409*, 318; c) A. Nilsson, L. G. M. Pettersson, *Nat. Commun.* **2015**, *6*, 8998; d) M. Falk, T. A. Ford, *Can. J. Chem.* **1966**, *44*, 1699; e) J. Russo, H. Tanaka, *Nat. Commun.* **2014**, *5*, 3556.
[8] R. Shi, H. Tanaka, *J. Am. Chem. Soc.* **2020**, *142*, 2868.
[9] C. D. S. Brites, B. Zhuang, M. L. Debasu, D. Ding, X. Qin, F. E. Maturi, W. W. Y. Lim, D. W. Soh, J. Rocha, Z. Yi, X. Liu, L. D. Carlos, *J. Phys. Chem. Lett.* **2020**, *11*, 6704.
[10] J. K. Gregory, D. C. Clary, K. Liu, M. G. Brown, R. J. Saykally, *Science* **1997**, *275*, 814.
[11] a) J. C. del Valle, E. Camarillo, L. Martinez Maestro, J. A. Gonzalo, C. Aragó, M. Marqués, D. Jaque, G. Lifante, J. G. Solé, K. Santacruz-Gómez, R. C. Carrillo-Torres, F. Jaque, *Philos. Mag.* **2015**, *95*, 683; b) L. M. Maestro, M. I. Marqués, E. Camarillo, D. Jaque, J. G. Solé, J. A. Gonzalo, F. Jaque, J. C. D. Valle, F. Mallamace, H. Stanley, *Int. J. Nanotechnol.* **2016**, *13*, 667.
[12] L. Labrador-Páez, E. Montes, M. Pedroni, P. Haro-González, M. Bettinelli, D. Jaque, J. García-Solé, F. Jaque, *J. Phys. Chem. C* **2018**, *122*, 14838.

[13] L. Labrador-Páez, D. J. Jovanović, M. I. Marqués, K. Smits, S. D. Dolić, F. Jaque, H. E. Stanley, M. D. Dramićanin, J. García-Solé, P. Haro-González, D. Jaque, *Small* **2017**, *13*, 1700968.
[14] Y. Shen, J. Lifante, N. Fernández, D. Jaque, E. Ximendes, *ACS Nano* **2020**, *14*, 4122.
[15] a) B. del Rosal, D. Ruiz, I. Chaves-Coira, B. H. Juárez, L. Monge, G. Hong, N. Fernández, D. Jaque, *Adv. Funct. Mater.* **2018**, *28*, 1806088; b) H. D. A. Santos, I. Zabala Gutiérrez, Y. Shen, J. Lifante, E. Ximendes, M. Laurenti, D. Méndez-González, S. Melle, O. G. Calderón, E. López Cabarcos, N. Fernández, I. Chaves-Coira, D. Lucena-Agell, L. Monge, M. D. Mackenzie, J. Marqués-Hueso, C. M. S. Jones, C. Jacinto, B. del Rosal, A. K. Kar, J. Rubio-Retama, D. Jaque, *Nat. Commun.* **2020**, *11*, 2933; c) D. Ruiz, B. del Rosal, M. Acebrón, C. Palencia, C. Sun, J. Cabanillas-González, M. López-Haro, A. B. Hungría, D. Jaque, B. H. Juarez, *Adv. Funct. Mater.* **2017**, *27*, 1604629; d) J. Lifante, Y. Shen, I. Zabala Gutierrez, I. Rubia-Rodríguez, D. Ortega, N. Fernandez, S. Melle, M. Granado, J. Rubio-Retama, D. Jaque, E. Ximendes, *Adv. Sci.* **2021**, *8*, 2003838.
[16] B. Wozniak, J. Dera, in *Light Absorption in Sea Water* (Eds: L. A. Mysak, K. Hamilton), Springer New York, New York, NY **2007**, p. 11.
[17] K. Ramasesha, L. De Marco, A. Mandal, A. Tokmakoff, *Nat. Chem.* **2013**, *5*, 935.
[18] a) D. Jaque, F. Vetrone, *Nanoscale* **2012**, *4*, 4301; b) D. Jaque, B. D. Rosal, E. M. Rodríguez, L. M. Maestro, P. Haro-González, J. G. Solé, *Nanomedicine* **2014**, *9*, 1047.
[19] Y. Shen, J. Lifante, I. Zabala-Gutierrez, M. de la Fuente-Fernández, M. Granado, N. Fernández, J. Rubio-Retama, D. Jaque, R. Marin, E. Ximendes, A. Benayas, *Adv. Mater.* **2022**, *34*, 2107764.
[20] Y. Zhang, Y. Liu, C. Li, X. Chen, Q. Wang, *J. Phys. Chem. C* **2014**, *118*, 4918.
[21] Y. Shen, J. Lifante, E. Ximendes, H. D. A. Santos, D. Ruiz, B. H. Juárez, I. Zabala Gutiérrez, V. Torres Vera, J. Rubio Retama, E. Martín Rodríguez, D. H. Ortgies, D. Jaque, A. Benayas, B. del Rosal, *Nanoscale* **2019**, *11*, 19251.
[22] C. D. S. Brites, S. Balabhadra, L. D. Carlos, *Adv. Opt. Mater.* **2019**, *7*, 1801239.
[23] Y. Shen, H. D. A. Santos, E. C. Ximendes, J. Lifante, A. Sanz-Portilla, L. Monge, N. Fernández, I. Chaves-Coira, C. Jacinto, C. D. S. Brites, L. D. Carlos, A. Benayas, M. C. Iglesias-de la Cruz, D. Jaque, *Adv. Funct. Mater.* **2020**, *30*, 2002730.
[24] a) J.-F. Zhu, Y.-J. Zhu, M.-G. Ma, L.-X. Yang, L. Gao, *J. Phys. Chem. C* **2007**, *111*, 3920; b) W. Yang, L. Zhang, Y. Hu, Y. Zhong, H. B. Wu, X. W. D. Lou, *Angew. Chem.* **2012**, *124*, 11669.